Full Paper

Wiley Online Library

ELECTROANALYSIS

DOI: 10.1002/elan.202060468

A Nanocomposite Containing Carbon Nano-onions and Polyaniline Nanotubes as a Novel Electrode Material for Electrochemical Sensing of Daidzein

Piotr Olejnik,*[a] Marianna Gniadek,[b] Luis Echegoyen,[c] and Marta E. Plonska-Brzezinska*[a]

Abstract: Glassy carbon electrode (GCE) were modified with nanocomposites containing conductive polyaniline nanotubes ($PANI_{nt}$) and carbon nano-onions (CNOs). Herein we report a simple and sensitive way for daidzein (DA) determination at concentrations between 1 and 10 μM by linear sweep voltammetry using GCE/$PANI_{nt}$/CNOs system. The DA electrochemical behavior was examined in two buffer environments (pH 7.5 and 4.5) using electrodes modified with the oxidized CNOs or their derivatives containing carboxyl and benzylamino functional groups. The direct electrooxidation of DA was observed at +0.65 V and +0.8 V at pH 7.5 and at +0.7 V and +1.1 V vs. Ag/AgCl at pH 4.5.

Keywords: daidzein detection · carbon nano-onions · electrochemical sensors · nanocomposite

1 Introduction

Currently, detection and quantification of daidzein (DA) as a naturally occurring pharmotherapeutic compound is very attractive due to its estrogen-like properties. DA, interchangeably called 7,4-dihydroxyisoflavone, shows low estrogenic activity, belonging to the group of phystoestrogene compounds [1–3]. As an individual representative of isoflavones, DA plays an important role in health protection and nutrition chemistry. It reveals antioxidant, antiallergic, antidiabetic and anticarcinogenic effects. DA molecules present in the human body may bind to the estrogenic and androgenic receptors and be responsible for female hormonal disorders and male prostate problems. Due to the ability to widen the coronary vessels, lower blood pressure, inhibit α-glucosidase activity and prevent arrhythmia, DA is used for the treatment of cardiovascular diseases, diabetes and menopause symptom amelioration [4–9]. DA occurs in varieties of leguminous plants (e.g., soybeans), which are members of the bean family, and is therefore present in all soy products such as milk or tofu, which makes DA an ingredient widely used in diets [10–14]. Due to its important role in human life and extensive range of properties, it is understandable and necessary to discover novel methods of DA detection and determination as well as to develop and improve the currently used methods. In the scientific literature, several methods of qualitative and quantitative DA analysis have been described.

The most common analysis methods include high-performance liquid and gas chromatography, which is most often combined with mass spectrometry and ultraviolet detection [15–17], enzyme-linked immunosorbent assay techniques [18] or methods based on the fluorescence resonance energy transfer effect [19]. DA molecules might be sensed using electrochemical methods by sensing devices. The electrochemical sensing devices provide advantages such as: low detection limits, a wide linear response range, long-term stability and reproducibility. The standard construction of electrochemical sensing systems assumes the presence of a transducer, which transforms the response into a detectable signal, and a chemically selective layer as a recognition part, which interacts with the target analyte and isolates the signal obtained as a result of chemical changes caused by the interaction [20]. When the chemically selective layer that is sensitive to the tested analyte, is not affected by other influences, the largest electrical conductivity is guaranteed to maximize the charge transfer rate to the electrode surface. Due to the high specific surface at the nanometer scale level and degree of coverage, the analytical signal is enhanced.

So far, recently found nanomaterials have the widest range of application in electrochemical sensor systems. Their high surface to volume ratio and above average dispersity directly improve the selectivity and sensitivity parameters [21]. Among the most studied and currently used nanomaterials in the electrochemical sensing field

[a] P. Olejnik, M. E. Plonska-Brzezinska
Faculty of Pharmacy with the Division of Laboratory Medicine, Medical University of Bialystok
Mickiewicza 2 A, 15-222 Bialystok, Poland
E-mail: polejnik@chem.uw.edu.pl
marta.plonska-brzezinska@umb.edu.pl
[b] M. Gniadek
Department of Chemistry, University of Warsaw
Pasteur 1, 02-093 Warsaw, Poland
[c] L. Echegoyen
Department of Chemistry, University of Texas at El Paso
500 W. University Ave., El Paso, TX79968

that meets the conditions of an ideally sensitive chemical layer are carbon-based ones.

Compared with other materials, carbonaceous nanostructures offer simple processes for manufacturing while maintaining a minimal number of defects. The most common carbon allotropes such as graphene, carbon nanotubes (CNTs), carbon dots, carbon nanofibers and nanodiamonds (NDs) provide chemical inertness, a relatively wide potential window, and low background currents; these allotropes are suitable for various analytes [22,23]. In their shade are still less popular structures resembling multi-layer fullerenes called carbon nano-onions (CNOs). The sensing ability of some of these carbon nanomaterials has been tested for DA detection. Liang et al. successfully applied graphene functionalized by poly(sodium 4-styrenesulfonate) for DA determination in human serum [24]. The SnO_2 decoration of graphene allows DA to be analyzed in a concentration range of 0.01–1 μM [25]. Ordered Langmuir-Blodgett films of CNTs modified by polyaniline provide good sensitivity towards DA on the level of 7.349 μA μM^{-1} [26]. This result confirms and is consistent with the fact that DA is a polyphenolic compound with phenolic hydroxyl groups, that can be easily oxidized. Unfortunately, the direct determination process of DA is characterized by a low values of analytical parameters. It might be caused by the high potentials required to initiate the redox reaction and results in background current increase and therefore sensitivity loss [28]. Additionally, DA is able to electropolymerize which may lead to electrode surface deactivation [29].

To overcome these disadvantages, there is still a need for novel sensing materials that increase the sensitivity and shorten the time of response. The combination of carbon nanomaterials with conducting polymers is very often used in the construction of electrochemical sensors. This combination significantly increases the specific surface area, induces high porosity, facilitates charge conduction, increases the number of active sites and improves the cycling stability [30–32]. Among the conductive polymer applied in the electrochemical sensing field, polyaniline stands out. The combination of PANI with CNOs is known in the scientific literature [33,34]. The replacement of macromolecular PANI by PANI nanotubes ($PANI_{nt}$) may offer advantages due to their good biocompatibility, high conductivity (up to six times higher from macromolecular PANI, for $PANI_{nt}$ with a diameter of 100 nm it is ca. 50 Scm^{-1}), high chemical stability, and ease and low cost of preparation. Recently, it has been proven that the composition $PANI_{nt}/CNOs_{ox}$ (oxidized form of CNOs) revealed a high specific capacitance of 950 $F g^{-1}$ [31]. Moreover, $PANI_{nt}$ is able to efficiently eliminate the impact of additional chemical interactions on the electrochemical response [35–37]. One of the most effective and simple methods of $PANI_{nt}$ production is chemical template synthesis. The use of an easily soluble matrix allows for the control of nanotubes size, which determines the final properties of the polymer [31,38,39]. Moreover, $PANI_{nt}$ conductivity can be enhanced by increasing the degree of nanostructured arrangement, with the most effective orientation being perpendicular to the surface [40].

Thus, the aim of this work was to establish a selective and sensitive electrochemical method for the detection and determination of DA using $PANI_{nt}/CNO$ nanocomposites as the sensing material. Most of the discussed nanocomposites include the $CNOs_{ox}$ due to the high efficiency of $CNOs_{ox}$ for DA electrochemical sensing.

2 Results and Discussion

2.1 Synthesis of Pristine Nanomaterials and their Composites, Spectroscopic and Microscopic Characterization

The synthesis of $PANI_{nt}$ was achieved using template method (Scheme 1A) proposed by Martin [36]. Polycarbonate (PC) membranes containing a 200 nm pore diameter were applied as matrices. The $PANI_{nt}$ fabricating step was achieved in 1 M sulfuric acid medium using ammonium persulfate as the oxidant for the aniline

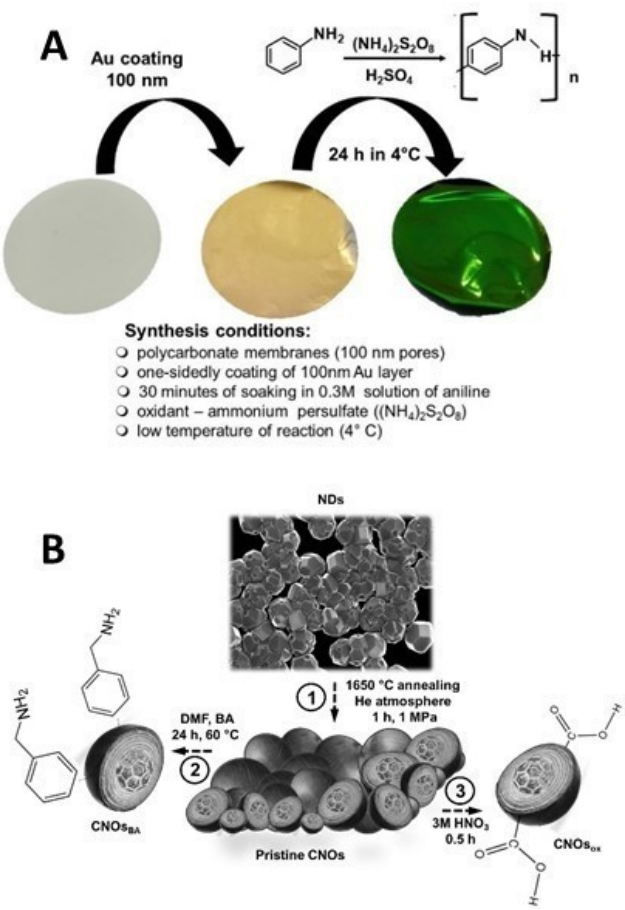

Scheme 1. (A) The simplified template synthesis of $PANI_{nt}$ and (B) modification procedure of the pristine CNOs, $CNOs_{ox}$ and $CNOs_{BA}$.

monomer. For the purposes of this experiment, PC membranes were coated one-sidedly with a few nanometers of uniform gold layer. The process was conducted by vapor deposition in a plasma sputter coater. The Au-covered templates were soaked 30 min in 5 mL of 0.3 M acidic aniline solution and then mixed with equivalent of 0.3 M oxidant in 1 M of sulfuric acid solution. The chemical polymerization process was performed at 4 °C for 3 h. After that, the membranes were removed by dissolving in chloroform solvent. The $PANI_{nt}$ anchored on thin gold layer were thoroughly rinsed using Milli-Q water.

Commercially available powder of nanodiamonds (NDs, Carbodeon Diamond®Molto, Vantaa, Finland) with a 4 to 6 nm crystal size and ND content >97 wt% was applied for fabricating the CNO spheres according to Kuznetsov's procedure [45]. NDs were placed in an Astro carbonization furnace and annealed at 1650 °C under a 1.1 MPa He atmosphere using a heating rate of 20 °C min^{-1}. The final temperature was maintained for 1 h. Next, the material was slowly cooled to room temperature, and the CNOs were annealed in air at 400 °C to eliminate amorphous structures (Scheme 1B).

The pristine CNOs oxidation was achieved by Lieber et al. procedure used for single CNTs [51]. The amount of 100 mg of pristine CNOs was 30 min ultrasonicated and refluxed for 48 h in 3.0 M aqueous nitric acid. After that, the mixture was centrifuged for 10 min followed by collection of the black precipitate that aggregated in the bottom of the test-tube. According to Salzmann's protocol $CNOs_{ox}$ were purified [52]. The $CNOs_{ox}$ were stirred in 3.0 M NaOH and rinsed several times using Milli-Q water until a final pH of 7 was reached, then the samples were dried overnight at 110 °C (Scheme 1B).

Further functionalization of the CNOs was conducted according to the procedure proposed by Giordani et al. [53]. Benzylamine and amyl nitrite were added to the pristine CNOs in DMF, and the reaction was performed under an inert N_2 atmosphere. The reaction was stirred overnight at 60 °C, and then the modified $CNOs_{BA}$ were separated from the reaction mixture by centrifugation (Scheme 1B).

Nanocomposite preparation was accomplished using the procedure briefly described below. In the first step, the template synthesis of $PANI_{nt}$ was accomplished using a PC membrane, which was thoroughly described previously (Scheme 1A). The $PANI_{nt}$/Au film was immediately immobilized on the GCE surface. Then, the $CNOs_{ox}$ were anchored onto the GC/Au/$PANI_{nt}$ electrode using aqueous solutions of carbodiimide (EDC) and N-hydroxysuccinimide (NHS) [31]. Briefly, 1 mg of $CNOs_{ox}$ was placed in a solution of 10 mM NHS and 40 mM EDC for 1 h. After the activation step, the $CNOs_{ox}$ were separated and dispersed in 1 mL of ethanol using an ultrasonic bath for 0.5 h to receive a black, homogeneous, and stable suspension. Finally, the activated $CNOs_{ox}$ suspension was immobilized onto GCE/Au/$PANI_{nt}$ surface, where amide bonds were formed, then the excess of unattached $CNOs_{ox}$ were also removed. The CNOs and $CNOs_{BA}$ were immobilized using simple physical adsorption on the GCE/Au/$PANI_{nt}$ surface by controlling the carbon nanostructure concentration in the solvent. The electrodes prepared in this way (GCE/Au/$PANI_{nt}$/CNOs, GCE/Au/$PANI_{nt}$/$CNOs_{ox}$ and GCE/Au/$PANI_{nt}$/$CNOs_{BA}$) were used as the working electrodes in the analyte determinations, and their performances were evaluated.

2.2 Spectroscopic and Microscopic Studies of $PANI_{nt}$/CNO Nanocomposites

Figure 1A shows the Raman spectrum of $CNOs_{ox}$ registered at 514 nm excitation. The spectrum exhibits four signals characteristic of carbon nanomaterials [41,42]. The signals are closely related to the hexagonal mode present in graphene and graphitic structures. The G band at a typical frequency of 1577 cm^{-1} is the best recognizable signal, and is due to the in-plane vibration of two related carbon atoms with sp^2 hybridization on the hexagonal ring in graphite [43,44]. The intensity and width of the G signal reflects the disorder of chains and hexagonal rings. The spectrum of CNOs is dominated by the D band occurring at 1340 cm^{-1}. Such a high intensity of the D band confirms the higher number of defects present on the outer graphitic layer, which in the case of $CNOs_{ox}$ is directly connected with the structural disorder caused by the presence of surface functional groups containing oxygen. Moreover, the D band corresponds to the presence of sp^3-hybridized carbon atoms.

Figure 1B shows the Raman spectrum for nanocomposites containing $PANI_{nt}$ and $CNOs_{ox}$. The characteristic signals for the carbon nanostructure are still clearly visible (D and G bands). The D/G intensity ratio decreases due to the high interference of the $PANI_{nt}$ signals between 1518–1622 cm^{-1}, that provide information about the stretching vibrations of C–C and C=C bonds. The additional bands derived from polymeric nanostructures appeared around 1170 and 1500 cm^{-1}, which are attributed to in-plane benzenoid ring bending and N–H bending, respectively [45].

The SEM images shown in Figure 2 confirm the formation of the nanocomposites containing $PANI_{nt}$ and CNOs on the polymeric nanotube's surface. The morphol-

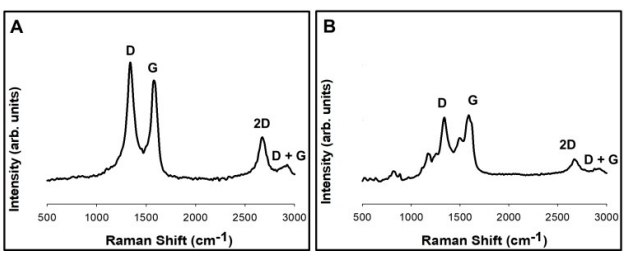

Fig. 1. Raman spectra of (A) $CNOs_{ox}$ on a GCE surface and (B) $PANI_{nt}$/$CNOs_{ox}$ nanocomposite on a GCE/Au surface recorded at 514 nm excitation.

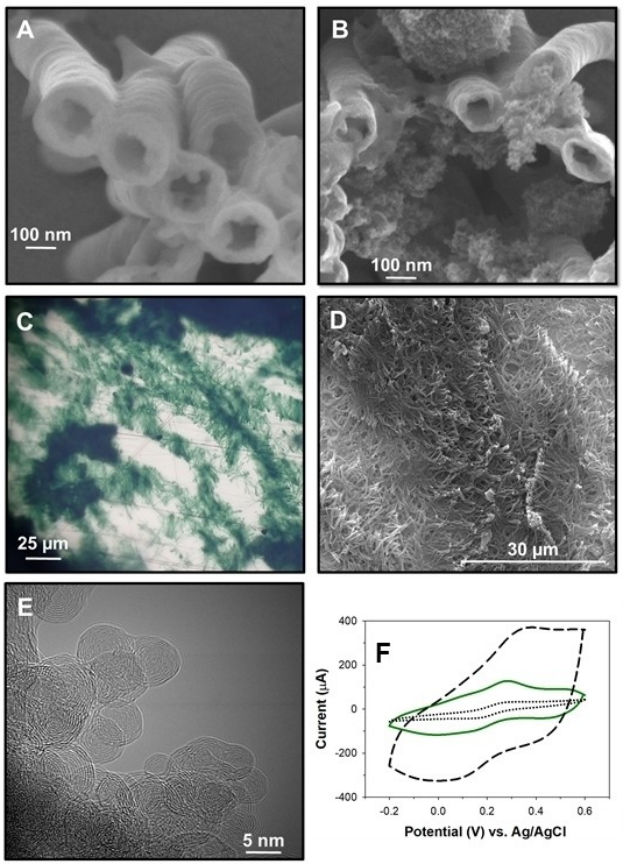

Fig. 2. SEM images of (A) pure $PANI_{nt}$ and (B) $PANI_{nt}/CNOs_{ox}$ nanocomposites on the GCE/Au surface. Pure $PANI_{nt}$ randomly oriented on the Au surface images captured by (C) optical microscopy in light field mode and (D) SEM. (E) HR-TEM image of $CNOs_{ox}$. (F) CVs for GCE/CNO_{ox} (pointed line), GCE/$PANI_{nt}$ (green line) and GCE/Au/$PANI_{nt}/CNOs_{ox}$ (dashed line) in the presence of 5 mM $Fe(CN)_6^{3-/4-}$ in 0.1 M PBS (pH = 7.4) at 50 mV s^{-1}.

ogies of $PANI_{nt}$ depend on the preparation conditions including the concentration of CNOs in the solution and type of CNOs. The thickness of the PC membrane and the diameter of the membrane pores define the $PANI_{nt}$ size. The average length and diameter of $PANI_{nt}$ is ca. 1 µm and 200 ± 30 nm, respectively. The pores density in the PC template reflects the distribution of $PANI_{nt}$ attached to the surface [31]. SEM images also confirmed that the polymeric nanotubes are empty inside. Our studies also indicate that the $PANI_{nt}$ extends perpendicularly to the surface, creating brush-like nanostructures (Figures 2C and 2D). As previously described, $PANI_{nt}$ forms on the Au surface (Figure 2A), and then the pristine CNOs or their derivatives are immobilized in a covalent or noncovalent manner on the GCE/Au/$PANI_{nt}$ surface. Figure 2B shows that the carbon nanostructures immobilized on $PANI_{nt}$. CNOs tend to aggregate, what is caused by van der Waals intermolecular forces between the nanoparticles, and it can be seen that the CNOs show a granular morphology. Figure 2E presents the high-resolution transmission electron microscopy (HR-TEM) for $CNOs_{ox}$ randomly dispersed on a copper mesh. For our studies, 5 nm, spherical CNO nanoparticles were used. After functionalization, the concentric graphitic layers of CNOs were not destroyed and no visible changes in the structure of the CNOs were observed.

2.3 Electrochemical Studies of $PANI_{nt}$/CNO Composites

Figure 2F shows cyclic voltammograms (CVs) registered in a model electrochemical system containing mixture of $Fe(CN)_6^{3-}/Fe(CN)_6^{4-}$ at a sweep rate 50 mV s^{-1}. The shape of recorded curves indicates that the layer of $PANI_{nt}$/CNO nanocomposite material is able to transfer the electrons in the electrode process. The $PANI_{nt}$ immobilized on the GC electrode surface affect the CVs shape but the distance between cathodic and anodic peaks increased slightly indicating good conductivity of the layer. To explore the potential application of $PANI_{nt}$/CNO composites for electrochemical sensing of DA, the synthesized samples were used as the working electrodes using CV in buffer solution at a sweep rate 100 mV s^{-1}. Figure 3 shows the electrochemical responses of the GCE/Au/$PANI_{nt}/CNOs$, GCE/Au/$PANI_{nt}/CNOs_{ox}$ and GCE/Au/$PANI_{nt}/CNOs_{BA}$ electrodes in the presence of the analyte (50 µM DA). To optimize the detection and determination of DA, the response of a GCE/Au/$PANI_{nt}$/

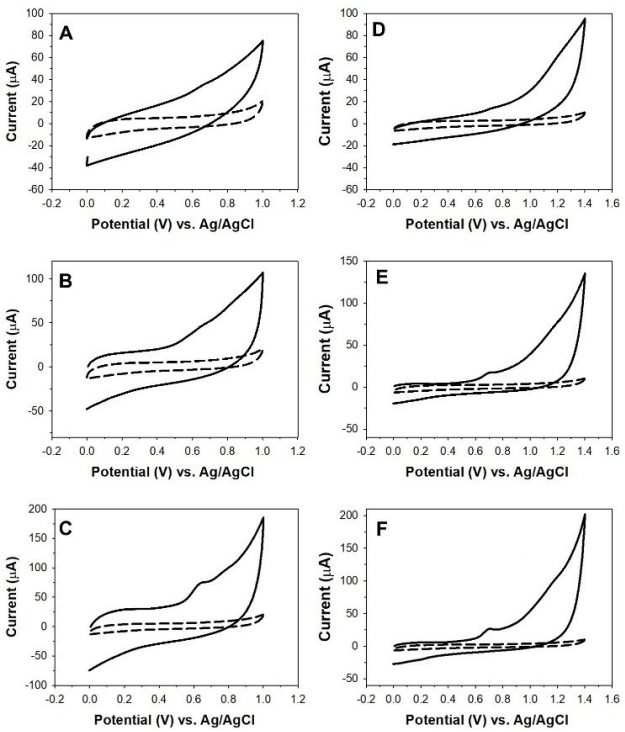

Fig. 3. The CV curves for 50 µM DA on (A) $PANI_{nt}/CNOs$, (B) $PANI_{nt}/CNOs_{BA}$, (C) $PANI_{nt}/CNOs_{ox}$ electrodes in 0.1 M PBS (pH = 7.4), (D) $PANI_{nt}/CNOs$, (E) $PANI_{nt}/CNOs_{BA}$, and (F) $PANI_{nt}/CNOs_{ox}$ electrodes in 0.1 M ABS (pH = 4.5) at 100 mV s^{-1}. Dashed curves represent nonmodified GCE.

CNOs electrode was investigated in the following buffer solutions: 0.1 M phosphate buffer (PBS) (pH 7.4) and 0.1 M acetate buffer (ABS) (pH 4.5). Regardless of the pH, the composite electrodes showed negligible activity towards DA. The highest electrode activity was registered for the $PANI_{nt}/CNOs_{ox}$ nanocomposite. The DA oxidation current increased for the applied nanostructured carbon electrodes in the following order: pristine CNOs < $CNOs_{BA}$ < $CNOs_{ox}$. According to the mechanism of the DA electrooxidation process proposed by Fernandes et al., the CVs should exhibit two consecutive, separated and irreversible characteristic peaks [46]. The peak clarity depends on the CNO derivative used. In the case of $PANI_{nt}$/CNO and $PANI_{nt}/CNO_{BA}$ electrodes, only one characteristic signal for DA electrooxidation at lower potential values is visible. The pair of redox peaks is visible on CV curves for the $PANI_{nt}/CNOs_{ox}$ nanocomposite. Its presence testifies to the higher efficiency and electron transfer rate of $CNOs_{ox}$, caused by electroactive functional groups abundant in oxygen atoms including free electron pairs that enhance the conductivity.

The potential of the DA the oxidation peaks is dependent on the pH value of the used electrolytes, see Figure 4. At a pH of 7.5, the first well-defined, characteristic oxidation signal occurs at +0.65 V vs. Ag/AgCl, which results from the effective electrochemical oxidation of DA. The second oxidation signal, at ca. +0.8 V, is barely visible in the presence of $CNOs_{ox}$. Similarly, in the case of a more acidic medium in 0.1 M ABS at pH 4.5, the characteristic signals for DA oxidation are well-resolved for the electrodes containing $CNOs_{ox}$. The peaks are shifted towards higher oxidation potential values at +0.75 and +1.1 V vs. Ag/AgCl. These results show that the oxidation process of DA on the $PANI_{nt}/CNOs_{ox}$ electrode is a function of the pH value and occurs at more positive potentials with increasing pH. The results for $PANI_{nt}$/$CNOs_{ox}$ indicate that PBS is a more suitable electrolyte due to the larger oxidation current. Therefore, the PBS solution was chosen as the supporting electrolyte for further analyses.

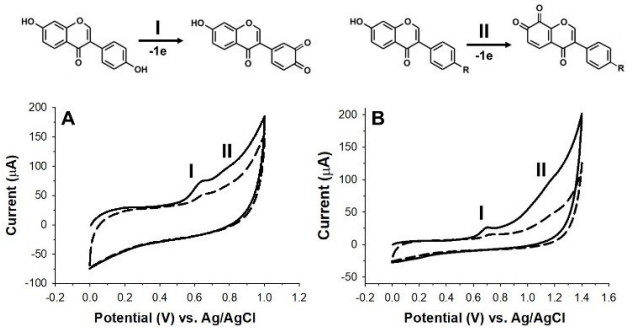

Fig. 4. The scheme of the DA electrooxidation process on $PANI_{nt}/CNOs_{ox}$ electrodes in (A) 0.1 M PBS, pH = 7.5 and (B) 0.1 M ABS, pH = 4.5 at 100 mV s^{-1} for 50 μM DA. The dashed curves represent the second cycle.

The CV studies clearly indicate that most of the hydroxyl functional groups present on the DA structure are electroactive (Figure 4). The DA molecule has two different –OH groups attached to benzene rings I and II. Based on the CVs, the hydroxyl groups attached to benzene ring I are easier to oxidize. In the second process, the less intense anodic peak II corresponds to the hydroxyl groups from benzene ring II at higher anodic potentials. The mechanism of both oxidation reactions assumes the creation of two transient, equal radical forms. Their presence allows for simultaneous oxidation of the DA molecules to quinone or to polymerization [47,48]. The DA polymerization process results in polymer product adsorption and rapid electrode surface passivation. This irreversible process is observed after the first cycle in Figure 4, where the dashed curves correspond to the less intense and developed second cycles of DA oxidation.

To understand the electrochemical response of DA on the $PANI_{nt}/CNOs$ electrode, the dependence of the catalytic current vs. sweep potential was examined (Figure 5). Due to the highest efficiency of the DA electrooxidation on the nanocomposite containing CNO_{ox} in 0.1 M PBS (pH 7.4), the GCE/Au/$PANI_{nt}/CNOs_{ox}$ electrode was chosen for further investigations. The CVs were registered at different sweep rates in the range between 40 and 300 mV s^{-1}. A linear dependence is observed for the relationship between the logarithm of anodic current (I_{pa}) and the logarithm of potential sweep rate (v) (Figure 5C), as described by the following equation:

$$\log I_{pa}(\mu A) = 0.8472 \log v\ \left(Vs^{-1}\right) - 0.3367 \qquad (1)$$

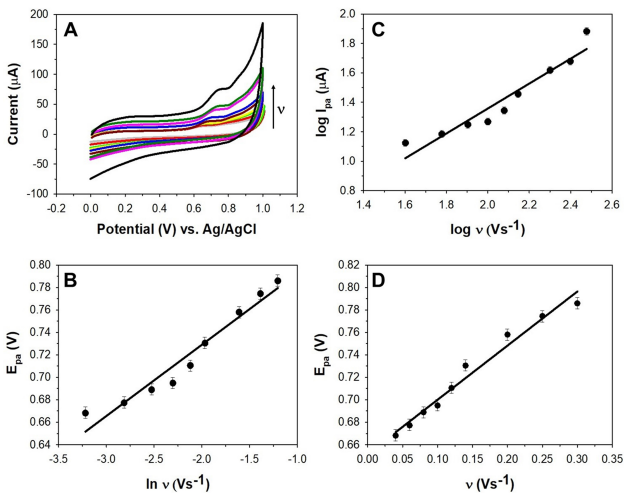

Fig. 5. (A) CVs for 50 μM DA in 0.1 M PBS, pH = 7.4 on the $PANI_{nt}/CNOs_{ox}$ at the different sweep rate: 40, 60, 80, 100, 120, 140, 200, 250, and 300 mV s^{-1}. (B) The linear dependence of DA oxidation peak potential (E_{pa}) vs. ln v. (C) The linear relationship between the logarithm of DA oxidation anodic current (I_{pa}) and the logarithm of the sweep rate. (D) The linear dependence of DA oxidation peak potential (E_{pa}) vs. potential sweep rate.

The theory for such linear dependence assumes that a slope value close to 0.5 corresponds to diffusion-controlled process; however, when the value is close to 1, it is due to an adsorption-controlled electrode process [49]. The slope for the dependence of this experiment is 0.8472, between 0.5 and 1.0, which suggests that the DA oxidation process is non-Fickian and results from simultaneous adsorption and diffusion processes. Figure 5B shows the linear relation between the potential of the anodic peak (E_{pa}) of the DA oxidation process and ln v. This dependence is expressed by:

$$E_{pa}\ (V) = 0.0635 \ln v\left(Vs^{-1}\right) + 0.8561 \quad (2)$$

where the slope is in accordance with the theory described by Laviron [50] and the following equation:

$$RT/\alpha NF = 0.0635 \quad (3)$$

where R is the gas constant (8.314 $J\,K^{-1}\,mol^{-1}$), F is the Faraday constant (96 487 C mol^{-1}), T is temperature (K), N is the number of transferred electrons, and α represents the charge transfer coefficient. Assuming that α = 0.5, N may be calculated as 0.8, which proves that the DA oxidation, according to the reaction schemes in Figure 4, is a one-electron process.

Assuming N to be 1, the experimental value of α is equal to 0.4. In accordance with the following equation [50]:

$$k_s = (1-\alpha)NFv/RT \quad (4)$$

Electrode reaction rate constant k_s for DA is calculated as $1.17 \pm 0.06\ s^{-1}$ and can be compared with k_s values for compounds from isoflavones group such as rutin ($1.59\ s^{-1}$) [51], puerarin ($1.72\ s^{-1}$) [52] or other with a similar structure like epinephrine ($1.35\ s^{-1}$) [53]. The formal standard potential for DA oxidation $E_{pa}{}^{o}$ (+ 0.65 V) was determined by extrapolation of the linear regression curve for the relation E_{pa} vs. v (Figure 5D).

DA oxidation on the $PANI_{nt}$/CNOs electrode is an irreversible process, so for further DA determination, linear sweep voltammetry (LSV) was performed. Figure 6A shows the superimposed curves illustrating the dependence between the anodic current for the oxidation peak and various concentrations of DA. The current of the DA oxidation signal increased linearly with DA concentration in the range of 1 to 10 μM (Figure 6B). The linear regression equation is:

$$I_{pa}\ (\mu A) = 1.828C\ (\mu M) - 1.412\ (R^2 = 0.9731) \quad (5)$$

with a detection limit of 0.77 ± 0.04 μM.

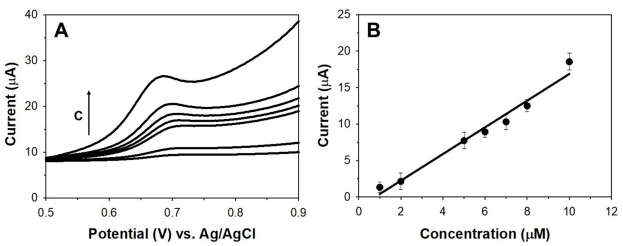

Fig. 6. LSV responses for the anodic peak of DA on the $PANI_{nt}$/$CNOs_{ox}$ electrode in 0.1 M PBS, pH = 7.4 at 0.1 $V\,s^{-1}$ for: 1, 2, 5, 6, 7, 8, 10 μM DA. (B). Linear dependence between Ip_a and concentration of DA.

Table 1 gives an overview regarding the DA determination using electrochemical sensors. According to the literature, the major disadvantages regarding these sensors are their low sensitivity and low stability, associated with the competitive adsorption and polymerization process of DA. The $PANI_{nt}$/$CNOs_{ox}$ electrode may be a competitive sensor, showing good sensitivity, enhanced electron transfer kinetics and a wide linear range of DA detection.

2.4 Reproducibility and Stability

The reproducibility was investigated for GCE/Au/$PANI_{nt}$/$CNOs_{ox}$ system in 0.1 M PBS at pH 7.4 in the presence of 5 μM DA. The experiment was carried out for three similarly prepared electrode. The relative standard deviation was calculated for DA oxidation current and equals 2.4 %. The experiment was repeated after 3 days and the slightly visible decrease of oxidation peak was observed. The results proves high reproducibility and stability of created electrochemical sensor.

3 Conclusion

A new class of biocompatible nanocomposites including $PANI_{nt}$ decorated with CNOs has been proposed as a promising material for electroactive determination of DA. The applied CNOs enhance the electron transfer between DA and GC surfaces, providing the ideal platform for enzymatic biocatalytic detection. The experiment also confirms that the DA oxidation process is irreversible and

Table 1. Comparison of electrochemical sensors for DA determination

Sensor	Sensitivity (μA μM^{-1})	Linear range (μM)	Detection limit (μM)	Ref.
GCE/MWCNTs [a]	1.479	6–100	0.72	[54]
GCE/MWCNTs-PANI-LB[b]	7.349	0.1–9	0.08	[26]
CPE/$ZrOCl_2$ [c]	1.739	0.03–2	0.01	[55]
GCE/SnO_2/PDDA-GR [d]	29.2	0.02–1	0.0067	[25]
GCE/$PANI_{nt}$/$CNOs_{ox}$ [e]	1.828	1–10	0.77	This work

[a] MWCNTs – multiwalled carbon nanotubes, GCE – glassy carbon electrode, [b] PANI-LB – polyaniline Langmuir-Blodgett layer, [c] CPE – carbon paste electrode, [d] PDDA – poly diallyldimethylammonium, GR – graphene, [a-e] DA determination was carried out using LSV technique.

requires only one electron per molecule. The good electrochemical response of $PANI_{nt}/CNO_{ox}$ towards DA and the linear dependence between the DA oxidation current and its concentration provide a simple and stable method for DA determination. In the future, the proposed method may also be applied for the determination of various phenolic biomolecules using in vivo and in vitro analyses.

4 Experimental Section

4.1 Materials

Aniline and sulfuric acid 96 % were supplied by POCh (Gliwice, Poland). The Whatman Nuclepore 200 nm polycarbonate (PC) membranes, synthetic 98 % DA (7,4-dihydroxyisoflavone), ammonium persulfate 98 % $(NH4)_2S_2O_8$, N-hydroxysuccinimide 98 % (NHS), and N-(3-dimethylaminopropyl)-N'-ethylcarbodiimide hydrochloride, commercial grade (EDC) were supplied by Sigma Aldrich (Buchs, Switzerland). A standard stock of the DA (1 mM) was prepared with ethanol and kept in the dark at 4 °C. Chloroform was obtained from Chempur Piekary Slaskie, Poland). The GC electrodes were polished using Texmet/alumina pads from a BASi PK-4 Polishing Kit. The 0.05 μm aluminum oxide powder was supplied by Buehler Micropolish (Esslingen, Germany). Used reagents were of analytical purity and applied as received. All supporting electrolyte solutions for electrochemical studies were prepared using deionized water, which was further purified with a Milli-Q system from Merck (Darmstadt, Germany).

4.2 Methods

The $PANI_{nt}$/CNOs nanocomposite layers were deposited on the surface of the GC and imaged using an FEI Tecnai S-3000 N (Tokyo, Japan) and a Merlin (Zeiss, Germany) field emission scanning electron microscope (FESEM). The structure of the CNOs was studied by a high-resolution transmission electron microscope (HR-TEM) system Libra 120 (Zeiss, Germany). The surface area of the nanocomposite and its organization were imaged and mapped by optical microscope HIROX KH-87000 (Tokyo, Japan).

Raman measurements were carried out by Renishaw Raman InVia Microscope (Wotton-under-Edge, United Kingdom) combined with a high-sensitivity ultralow-noise Charge Coupled Device (CCD) detector and a microstage for sample analysis using reflective method. The experiment was conducted with Ar ion laser with an excitation of 514 nm. Three scans, with a duration of 10 s each, were registered at the spectral resolution of 4 cm^{-1} and averaged to receive a single spectrum.

The electrochemical responses were collected by AUTOLAB (Utrecht, The Netherlands) potentiostat/galvanostat using the NOVA AUTOLAB software (Utrecht, The Netherlands). The measurements were carried out using three-electrode system consisting of a working GC disk electrode (2 mm diameter), an Ag/AgCl reference electrode (with saturated KCl), and the auxiliary Pt electrode. The geometrical surface area of the GC working electrode was estimated to be about 0.0314 cm^2. The GC electrode was mirror-polished using 0.5 micron alumina oxide powder on an alumina polishing pad and rinsed repetitively with Milli-Q water and ethanol before use. All electrochemical experiments were carried out under anaerobic conditions at room temperature (23 °C). The dissolved oxygen was removed from the measuring cell by Ar-purging within 15 min

Acknowledgements

The authors thank the National Science Center (NSC), Poland, for the generous support of this work: #2016/20/S/ST5/00371 to P.O. L.E. thanks the United State National Science Foundation (NSF) for generous support under CHE-1801317 and to the Robert A. Welch Foundation for an endowed chair (grant AH-0033).

Data Availability Statement

The author confirm that the data supporting the findings of this study is available within the article.

References

[1] M.-Y. Sun, Y. Ye, L. Xiao, K. Rahman, W. Xia, H. Zhang, *Afr. J. Tradit. Complement. Altern. Med.* **2016**, *13*, 117–132.
[2] M. Satterfield, D. M. Black, J. S. Brodbelt, *J. Chromatogr. B* **2001**, *759*, 33–41.
[3] S. Poschner, A. Maier-Salamon, M. Zehl, J. Wackerlig, D. Dobusch, B. Pachmann, K. L. Sterlini, W. Jäger, *Front. Pharmacol.* **2017**, *8*, DOI 10.3389/fphar.2017.00699.
[4] Y. Gao, W. Gu, L. Chen, Z. Xu, Y. Li, *Biomaterials* **2008**, *29*, 4129–4136.
[5] C. Picherit, V. Coxam, C. Bennetau-Pelissero, S. Kati-Coulibaly, M.-J. Davicco, P. Lebecque, J.-P. Barlet, *J. Nutr.* **2000**, *130*, 1675–1681.
[6] Z.-M. Liu, S. C. Ho, Y.-M. Chen, B. Tomlinson, S. Ho, K. To, J. Woo, *Eur. J. Clin. Nutr.* **2015**, *69*, 1161–1168.
[7] M.-H. Park, J.-W. Ju, M. Park, J. Han, *Eur. J. Pharmacol.* **2013**, *712*, 48–52.
[8] M. Liu, N. Yanagihara, Y. Toyohira, M. Tsutsui, S. Ueno, Y. Shinohara, *Endocrinology* **2007**, *148*, 5348–5354.
[9] P. Rivera, M. Pérez-Martín, F. J. Pavón, A. Serrano, A. Crespillo, M. Cifuentes, M.-D. López-Ávalos, J. M. Grondona, M. Vida, P. Fernández-Llebrez, F. R. de Fonseca, J. Suárez, *PLoS One* **2013**, *8*, DOI 10.1371/journal.pone.0064750.
[10] P. B. Kaufman, J. A. Duke, H. Brielmann, J. Boik, J. E. Hoyt, ***J***. *Altern. Complement. Med.* **1997**, *3*, 7–12.
[11] R. Laurenz, P. Tumbalam, S. Naeve, K. D. Thelen, *J. Sci. Food Agric.* **2017**, *97*, 3342–3347.
[12] J. O. Bennett, O. Yu, L. G. Heatherly, H. B. Krishnan, *J. Agric. Food Chem.* **2004**, *52*, 7574–7579.
[13] W. Chen, X. Ma, Y. Lin, Y. Xiong, C. Zheng, Y. Hu, D. Yu, Z. Jiang, *J Anim Sci Biotechnol* **2016**, *7*, DOI 10.1186/s40104-016-0102-z.

[14] J. Liggins, L. J. C. Bluck, S. Runswick, C. Atkinson, W. A. Coward, S. A. Bingham, *J. Nutr. Biochem.* **2000**, *11*, 326–331.
[15] B. F. Thomas, S. H. Zeisel, M. G. Busby, J. M. Hill, R. A. Mitchell, N. M. Scheffler, S. S. Brown, L. T. Bloeden, K. J. Dix, A. R. Jeffcoat, *J. Chromatogr. B* **2001**, *760*, 191–205.
[16] A. Aresta, P. Cotugno, F. Massari, C. Zambonin, *J. Food Qual.* **2017**, *2017*, 1-5..
[17] S. L. Pumford, M. M. Morton, A. Turkes, K. Griffiths, *Ann. Clin. Biochem.* **2002**, *39*, 281–292.
[18] C. Bennetau-Pelissero, B. Arnal-Schnebelen, V. Lamothe, P. Sauvant, J. L. Sagne, M. A. Verbruggen, J. Mathey, O. Lavialle, *Food Chem.* **2003**, *82*, 645–658.
[19] A. B. Dumbrepatil, S.-G. Lee, S. J. Chung, M. G. Lee, B. C. Park, T. J. Kim, E.-J. Woo, *Analyst* **2010**, *135*, 2879–2886.
[20] D. W. Kimmel, G. LeBlanc, M. E. Meschievitz, D. E. Cliffel, *Anal. Chem.* **2012**, *84*, 685–707.
[21] G. Maduraiveeran, W. Jin, *Trends Environ. Anal. Chem.* **2017**, *13*, 10–23.
[22] A. C. Power, B. Gorey, S. Chandra, J. Chapman, *Nanotechnol. Rev.* **2018**, *7*, 19–41.
[23] F. R. Baptista, S. A. Belhout, S. Giordani, S. J. Quinn, *Chem. Soc. Rev.* **2015**, *44*, 4433–4453.
[24] Y. Liang, C. Qu, R. Yang, L. Qu, J. Li, *Sens. Actuators B* **2017**, *251*, 542–550.
[25] Y. Fu, L. Wang, Y. Duan, L. Zou, B. Ye, *Talanta* **2017**, *168*, 1–9.
[26] L. Wang, Y. Li, Q. Wang, L. Zou, B. Ye, *Sens. Actuators B* **2016**, *228*, 214–220.
[27] "Electrochemical Behaviours of Daidzein at Multi-Wall Carbon Nanotubes Modified Glassy Carbon Electrode," can be found under http://connection.ebscohost.com/c/articles/89561012/electrochemical-behaviours-daidzein-multi-wall-carbon-nanotubes-modified-glassy-carbon-electrode, **n.d**.
[28] A. D'Antuono, V. C. Dall'Orto, A. L. Balbo, S. Sobral, I. Rezzano, *J. Agric. Food Chem.* **2001**, *49*, 1098–1101.
[29] S. Fletcher, V. J. Black, *J. Phys. Chem. C* **2016**, *120*, 8014–8022.
[30] A. N. Papathanassiou, M. E. Plonska-Brzezinska, O. Mykhailiv, L. Echegoyen, I. Sakellis, *Synth. Met.* **2015**, *209*, 583–587.
[31] P. Olejnik, M. Gniadek, L. Echegoyen, M. E. Plonska-Brzezinska, *Polymer* **2018**, *10*, 1408.
[32] M. O. Ansari, in *Electrically Conductive Polymer and Polymer Composites*, John Wiley & Sons, Ltd, **2018**, pp. 69–91.
[33] M. E. Plonska-Brzezinska, J. Mazurczyk, B. Palys, J. Breczko, A. Lapinski, A. T. Dubis, L. Echegoyen, *Chem. Eur. J.* **2012**, *18*, 2600–2608.
[34] A. Łapiński, A. T. Dubis, M. E. Plonska-Brzezinska, J. Mazurczyk, J. Breczko, L. Echegoyen, *Phys. Status Solidi C* **2012**, *9*, 1210–1212.
[35] M. Khalid, M. A. Tumelero, I. S. Brandt, V. C. Zoldan, J. J. S. Acuña, A. A. Pasa, *Indian Journal of Materials Science* **2013**, *2013*, 1–7.
[36] C. R. Martin, *Acc. Chem. Res.* **1995**, *28*, 61–68.
[37] F. Ran, Y. Tan, J. Liu, L. Zhao, L. Kong, Y. Luo, L. Kang, *Polym. Adv. Technol.* **2012**, *23*, 1297–1301.
[38] P. Olejnik, M. Gniadek, B. Palys, *J. Phys. Chem. C* **2012**, *116*, 10424–10429.
[39] P. Liu, Y. Zhu, J. Torres, S. H. Lee, M. Yun, *J. Polym. Sci. Part A* n.d., *55*, 3973–3979.
[40] L. Li, J. Qiu, S. Wang, *Electrochim. Acta* **2013**, *99*, 278–284.
[41] K. Sattler, Ed., *Carbon Nanomaterials Sourcebook: Graphene, Fullerenes, Nanotubes, and Nanodiamonds, Volume I*, CRC Press, **2016**.
[42] D. Roy, M. Chhowalla, H. Wang, N. Sano, I. Alexandrou, T. W. Clyne, G. A. J. Amaratunga, *Chem. Phys. Lett.* **2003**, *373*, 52–56.
[43] A. C. Ferrari, *Solid State Commun.* **2007**, *143*, 47–57.
[44] S. Reich, C. Thomsen, *Philos. Trans. R. Soc. London Ser. A* **2004**, *362*, 2271–2288.
[45] M. E. Plonska-Brzezinska, A. Molina-Ontoria, L. Echegoyen, *Carbon* **2014**, *67*, 304–317.
[46] I. P. G. Fernandes, S. C. B. Oliveira, M. Ghalkhani, S. Shahrokhian, M. Oliveira-Brett, **n.d.**, 9.
[47] N. Belhadj Tahar, A. Savall, *Electrochim. Acta* **2009**, *55*, 465–469.
[48] M. Ghalkhani, I. P. G. Fernandes, S. C. B. Oliveira, S. Shahrokhian, A. M. Oliveira-Brett, *Bioelectrochemistry* **2011**, *80*, 175–181.
[49] K. Suliborska, M. Baranowska, A. Bartoszek, W. Chrzanowski, J. Namieśnik, *Proceedings* **2019**, *11*, 23.
[50] E. Laviron, *J. Electroanal. Chem. Interfacial Electrochem.* **1979**, *101*, 19–28.
[51] D. Miao, J. Li, R. Yang, J. Qu, L. Qu, P. de B Harrington, *J. Electroanal. Chem.* **2014**, *732*, 17–24.
[52] S. Jing, H. Zheng, L. Zhao, L. Qu, L. Yu, *Talanta* **2017**, *174*, 477–485.
[53] R. Sadhana, P. A. Vidyadharan, A. Vidyadharan, "Solar Exfoliated Graphene Oxide: A Platform for Electrochemical Sensing of Epinephrine," **2020**.
[54] Z. Cai, J. N. Gan, D. F. Lu, X. Zhang, *Asian J. Chem.* **2012**, *24*, 4986–4990.
[55] Y. Li, Y. Li, J. Gao, L. Wang, L. Zou, B. Ye, *Electroanalysis* **2015**, *27*, 1719–1725.

Received: September 9, 2020
Accepted: December 13, 2020
Published online on ■■, ■■

FULL PAPER

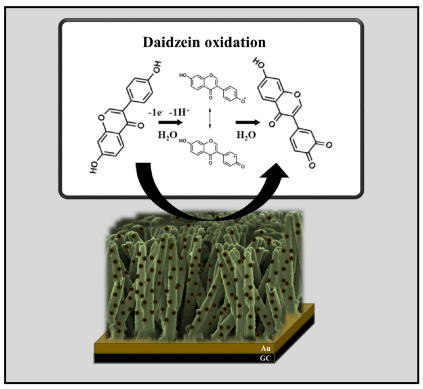

P. Olejnik, M. Gniadek, L. Echegoyen, M. E. Plonska-Brzezinska**